Structure and electronic properties of biomorphic carbon matrices and SiC ceramics prepared on their basis

A. A. Konchits,[1] B. D. Shanina,[1] S. V. Krasnovyd,[1,a)] V. O. Yukhymchuk,[1] O. M. Hreshchuk,[1] M. Ya. Valakh,[1] M. A. Skoryk,[2] S. A. Kulinich,[3] A. E. Belyaev,[1] and D. A. Iarmolenko[1]

[1]*V. Lashkaryov Institute of Semiconductor Physics, National Academy of Science of Ukraine, Prospect Nauky, 41, Kyiv 03028, Ukraine*
[2]*Nanomedtech LLC, Antonovych St., 68, Kyiv 03680, Ukraine*
[3]*Research Institute of Science and Technology, Tokai University, Hiratsuka, Kanagawa 259-1292, Japan*

(Received 5 June 2018; accepted 11 September 2018; published online 5 October 2018)

Biomorphic carbon matrices (BCMs) were produced by pyrolysis from wood species of different forest and garden trees, after which the as-prepared BCMs were converted to SiC ceramics through their impregnation with liquid silicon and further heat-treatment. Both types of obtained samples were studied by scanning electron microscopy (SEM), Raman scattering (RS), and electron spin resonance (ESR) methods. The SEM data reveal that all BCM samples contain large (10–50 μm) and small (1–5 μm) micro-pores with surface densities $\sim 10^9$ m^{-2} and 10^{11} m^{-2}, respectively. Analysis of RS allowed to estimate carbon cluster sizes of about 5–11 nm depending on the sample type. The study of the electronic structure using ESR spectroscopy is carried out for BCM and SiC ceramics samples. Using theoretical analysis of the ESR spectra, it was found that spin resonance in BCMs is due to the contribution of three spin systems: free electron spins, "pseudo-free" electron spins from the tail of density states below the conduction band, and localized spins at dangling carbon bonds (DCBs). Their contributions depend on the ratio of different structural phases such as sp^2-hybridized graphite-like carbon network and amorphous carbon phase. For most BCM samples, the large ESR line width is dramatically narrowed when samples are pumped out due to the exclusion of the broadening effect of molecular oxygen. The transformation of BCM into SiC by impregnation with liquid silicon can be clearly traced in the Raman spectra and in the ESR spectra. It is established that the electronic properties of synthesized SiC ceramics are due to the presence of residual graphite-like carbon nanoclusters. *Published by AIP Publishing.* https://doi.org/10.1063/1.5042844

I. INTRODUCTION

Nowadays, due to their numerous attractive properties, carbon-based materials are extensively studied and used in diverse fields of human activities.[1] Among other materials, those produced via pyrolysis from various organic objects have been actively studied and developed over the last decade.[2] A great deal of attention paid to such structures is explained by a number of important, and often unique, characteristics demonstrated by these materials. Firstly, such materials are pseudomorphic to their original biological objects at the micro-, meso-, and macroscales. Secondly, the properties of pyrolyzed materials, such as density, specific surface area, mechanical characteristics, electrical and thermal conductivities, as well as the pore hierarchy, are significantly different from their precursors.[3,4]

Biomorphic carbon matrices (BCMs) can be used for further fabrication of biomorphic SiC ceramics,[3–5] as well as for electromagnetic interference shielding,[6] as efficient support for nanocatalysts,[7] as filters for gas and liquids,[8,9] as a material for field emitters,[10] as sensors of harmful elements accumulated in the initial wood from which the carbon material was made,[11] as electrodes in lithium batteries and supercapacitors,[12,13] in medicine for the adsorption of harmful substances in human body,[14] for the formation of hydrophobic carbon surfaces,[15] bioimplants,[16] and so on. For each of the above applications, the biomorphic carbon-based material should be produced from a carefully selected precursor plant with optimal characteristics, including the necessary pore hierarchy.

The present work aimed at studying structural, morphological, and electronic properties of BCMs produced via pyrolysis of different species of wood, as well as SiC ceramics prepared on their basis. So far, there was no systematic research of the BCMs' electronic properties as well as the influence of the BCMs' structure peculiarity on the final ceramic product. It is necessary to clarify how BCM properties depend on the type of wood and its porosity, hardness, relation between closed and opened pores, and so on. It is necessary to study the peculiarities of electronic structure of these materials to clarify the type of the interatomic bonds in produced BCMs and SiC ceramics. The work thus establishes direct links between the morphology of precursor wood, treatment conditions for BCMs, and the properties of the final product in the chain: wood-BCM-SiC ceramics. The structure of this paper is given as follows: Sec. II gives information about methods of study and the necessary characteristics

a)Author to whom correspondence should be addressed: sergkrasnovyd88@gmail.com

TABLE I. Parameters of Raman bands (frequencies, widths, and intensities) and the ratios of integral intensities I_D/I_G, I_D/I_{D3}, I_D/I_{D4} for different BCM samples, and the sizes of carbon clusters (L_a) in them. (The abbreviations for BCM samples are listed in Sec. II, item: samples.)

BCM sample	ν_D (cm^{-1})	Γ_D (cm^{-1})	ν_G (cm^{-1})	Γ_G (cm^{-1})	ν_{D3} (cm^{-1})	Γ_{D3} (cm^{-1})	ν_{D4} (cm^{-1})	Γ_{D4} (cm^{-1})	ν_D (cm^{-1})	Γ_D (cm^{-1})	I_D/I_G	I_D/I_{D3}	I_D/I_{D4}	L_a (nm)
Ch	1368	99	1594	53	1529	145	1296	30	1620	50	1.07	12.71	2.13	9.7
O	1364	121	1594	51	1530	159	1279	41	1620	48	1.78	11.61	1.82	5.8
P	1368	60	1590	45	1475	227	1289	60	1620	42	0.95	20.7	6.01	10.9
M	1365	113	1594	49	1516	144	1272	86	1621	47	1.65	4.61	1.49	6.3
C	1367	111	1596	48	1525	152	1282	67	1620	40	1.55	11.55	1.94	6.7
L	1368	123	1594	56	1517	146	1276	48	1617	53	1.52	10.16	1.6	6.8
S	1364	121	1595	53	1537	183	1266	66	1620	47	1.44	15.61	2.02	7.2
A	1367	123	1596	55	1525	146	1277	54	1618	48	1.52	14.08	1.97	6.8

and designations of samples under study; Sec. III represents the SEM, Raman, and ESR experimental results for BCM structures as well as their discussion; in Sec. IV are described properties of the produced SiC ceramics; conclusions of total research are given in Sec. V.

II. METHODS AND EXPERIMENTAL

A. Methods

The technology for the production of BCMs from different types of plants (forest and garden trees) consists in carrying out pyrolysis in an inert atmosphere of properly shaped cut pieces of wood. For this, preforms of different breeds of trees were heated for 6–8 h in a horizontal quartz tube in an Ar flow (the flow rate being ~10 cm^3/min). To avoid the destruction of the internal structure of samples at high temperatures, the initial stage of pyrolysis was carried out quite slowly (1–2 °C/min). After reaching the temperature of 400 °C, the heating rate was increased to 5–6 °C/min. After reaching 900 °C, the temperature was stabilized. The specimens were kept at this temperature for 1 h, after which the system was slowly cooled down to room temperature.

To transform the prepared BCMs to porous SiC ceramics, the former were impregnated with liquid silicon, which led to the synthesis of SiC. The reaction can be represented as $C_{sol} + Si_{liq} \rightarrow SiC_{sol}$. The process was carried out in two stages. First, carbon crucibles with BCM were heated at low Ar pressure (200–300 mbar) to a temperature of T ≈ 1450–1550 °C for 20 min. Then, argon was pumped out and the temperature was raised to T ≈ 1750–1950 °C for 120 min. For the formation of stoichiometric SiC, the ratio of the initial components ψ = C/Si had to be 2.33. The residual carbon in the samples was destroyed in the process of its combustion under an atmosphere of oxygen at a temperature of 800 °C.

The morphology of the obtained BCMs was investigated using scanning electron microscopy (SEM, Tescan Mira 3 MLU). The local structure of BCMs and SiC samples was studied by Raman spectroscopy (Micro-Raman spectrometer JobinYvon T64000) at room temperature; a solid state-laser with a wavelength of 457 nm was used as an excitation source. To study the electronic properties of the prepared materials, electron spin resonance (ESR) measurements were carried out at room temperature using an X-band ESR spectrometer (Radiopan X-2244) with 100 kHz modulation of magnetic field. The estimated accuracy in the determination of the g-factor was $\pm(1–5) \times 10^{-4}$, depending on the ESR line width. The spin concentration N_s was estimated using a reference sample of MgO: Cr^{3+} (number of spins $N_{Cr} = 2 \times 10^{14}$). The accuracy of the N_s determination was ±50%.

TABLE II. ESR characteristics of the BCM samples of different plant origin.

BCM sample	S	P	C	Ch	M	O_{branch}	$O_{sapwood}$	L	A
On air									
ΔB_{ce} (mT)[a]	11.6	3.5	11.5	14.3	40.5	25.0	≈70	13.0	14.0
ΔB_{lc} (mT)	…	…	…	…	81	…	…	…	…
g_{ce}	2.004	2.009	2.026	1.9974	2.27	1.97	≈2.0	1.94	2.00
g_{lc}	…	…	…	…	1.996	…	…	…	…
N_{ce} (10^{17} cm^{-3})	6	5.8	8.4	32	90	3	≈2.0	5	4.8
N_{lc} (10^{17} cm^{-3})	…	…	…	…	2.7	…	…	…	…
Under vacuum									
ΔB_{ce} (mT)	4.4	2.5	1.6	1.07	0.5	0.6	≈48	0.51	0.38
ΔB_{lc} (mT)	…	3.9	3.6	1.07	0.71	2.0	…	…	…
g_{ce}	2.0074	2.0064	2.0016	2.0042	2.0036	2.003	≈2.0	2.0029	2.0006
g_{lc}	…	2.007	2.04	2.0165	2.0061	2.003	…	…	…
N_{ce} (10^{17} cm^{-3})	11.8	3.3	10.8	8.9	22.4	0.8	≈2.0	3.8	3.9
N_{lc} (10^{17} cm^{-3})	…	0.41	1.05	3	1.24	0.1	…	…	…

[a]The subscripts "*ce*" and "*lc*" refer to the conduction electrons and localized centers, respectively.

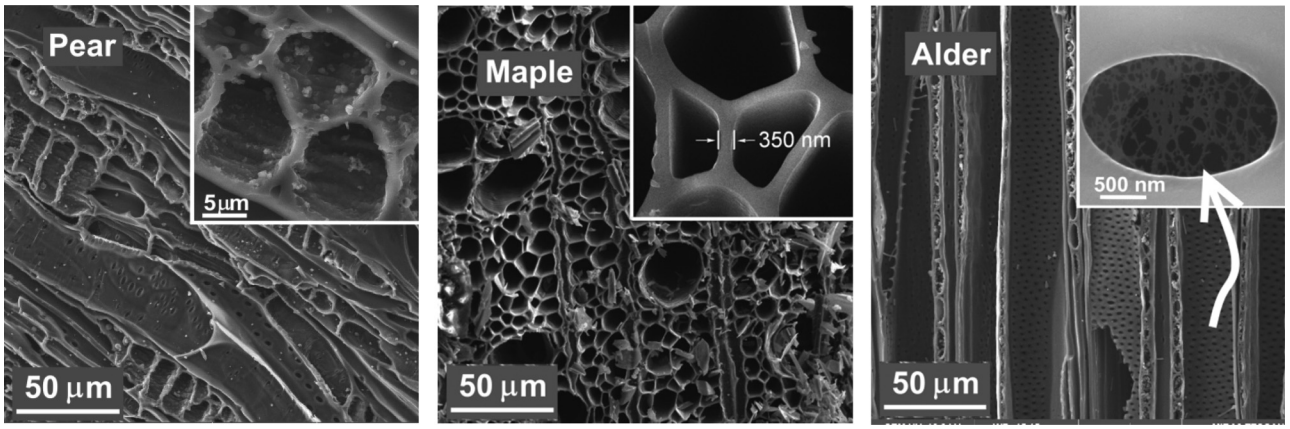

FIG. 1. SEM images of some carbon-based matrices pyrolysis-produced from different wood species. View along the pores: pear- and alder-derived BCMs. View normal to fiber direction: maple derived BCM. Insets show enlarged images of the same structures.

B. Samples

Although the measurements in this study were done for a lot of BCMs derived from different wood species, eight of them were selected as a presentative of wood specimens with different densities, hardness, and porosities. The main designation of those BCM samples is connected with the corresponding wood which the BCM is derived from. These are the samples: S is sea-buckthorn-derived BCM; P is pear-derived one; C is cornel-derived; Ch is cherry plum-derived; M is maple-derived; O is oak-derived; L is linden-BCM; A is alder-BCM. These designations are used in Tables I and II. For the production of the SiC ceramics only samples of alder and pear BCMs with the best porosity were selected. The numeration of these SiC ceramic samples is Ac and Pc, where "c" means ceramics. For pear-derived SiC ceramics three samples (Pc1, Pc2a, and Pc2b) differing in the synthesis temperature and the distance from the surface of one large piece of SiC ceramic from which samples Pc2a and Pc2b were cut out (see Sec. IV) were studied. To control the homogeneity of the properties of SiC ceramics, a brief comparative study of ESR and Raman scattering was also carried out on additional Pc2c-Pc2f samples cut from the same large piece of ceramics as the samples of Pc2a and Pc2b.

III. PROPERTIES OF BCMS: RESULTS AND DISCUSSION

A. Morphology of specimens

In the current work, numerous BCM samples from various species of forest and garden trees were produced and investigated (see Table I). In the process of pyrolysis at temperatures exceeding 600 °C, such components as H_2O, CO_2, acids, carbonyl groups, and alcohols are known to be removed from the sample after decomposition of its organic substances.[3,4] The main organic compounds that constitute the walls of the wood framework are transformed into the carbon framework which is pseudomorphic to the parent structure of the tree material.[3,4] Figure 1 presents, for example, SEM images of BCMs obtained from pear, maple, and alder. The pear- and alder-derived BCMs are fractured along their wood fibers, the maple-derived BCMs were cut normal to their fiber directions. As it is clearly seen in Fig. 1, there are visible micro-pores with diameters of 10–50 μm, and surface density of $(4–6)\times10^9$ m^{-2}, and micro-pores with diameters of 1–5 μm and a surface density of $(1–2)\times10^{11}$ m^{-2}.

As seen in the SEM images in Fig. 1, all pyrolysis-produced samples exhibited thick dense walls and voids, which in turn had nano-scaled pipes, pores, and wires. The walls of such as-prepared networks have different thicknesses, from tens of nm to micrometers.

B. Raman spectroscopy characterization of BCMs

Figure 2(a) presents Raman spectra of the BCM samples studied. Qualitatively, all the spectra in Fig. 2(a) are typical of nanocrystalline carbon.[17] For convenience, in all spectra, the base line was subtracted from photoluminescence (PL) and the intensities of all bands were normalized to the intensity of the G-band. All the BCM Raman spectra, except the pear-based BCM, are quite similar. The differences in the spectra are only in their intensities in the regions of D_4

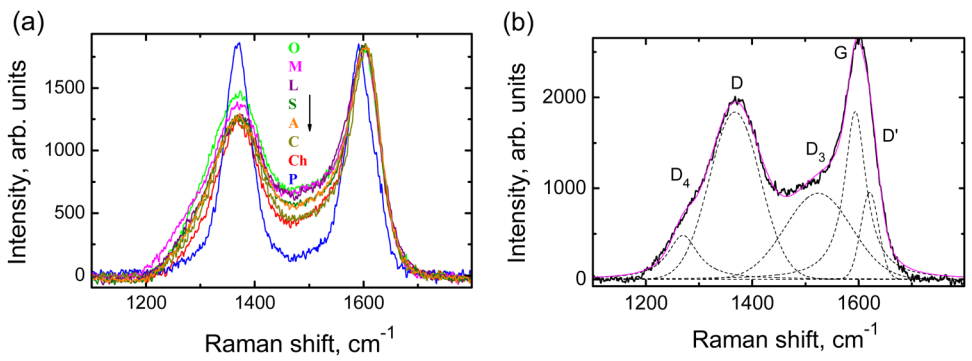

FIG. 2. (a) Raman spectra of BCMs derived from different wood species. (b) Spectrum of maple-based BCM deconvoluted into five components: D_4, D, D_3, G, and D′.

(1250 cm^{-1}), D_3 (1500 cm^{-1}), and D (1350 cm^{-1}) bands. For quantitative comparison, all the spectra in Fig. 2(a) were deconvoluted into five components corresponding to the following bands: D (also called D_1), D′(also called D_2), D_3, D_4, and G [see Fig. 2(b) as an example].

The so-called G-band (emerging in the region 1580–1590 cm^{-1}) is well-known as a manifestation of any carbon-based material in its first-order Raman spectrum.[18] It is related to the double degenerate mode of E_{2g}-symmetry for the center of the Brillouin zone and results from tensile vibrations of all pairs of carbon atoms that have sp^2-hybridization and form benzene rings.[18] The presence of defects in carbon structures is known to result in bands D (~1350 cm^{-1}) and D′ (1620 cm^{-1}). The D-band is a manifestation of the A_{1g} breathing mode activated by defects at the point K of the Brillouin zone of sp^2-hybridized carbon atoms.[19] This band is only observable in Raman spectra of samples with defects, since it is forbidden by selection rules in defect-free structures. For the same reason, the presence of defects is also a condition for the observation of the band D′ (1620 cm^{-1}). At the same time, the nature of vibrations giving rise to the D′-band differs from that of vibrations resulting in the D-mode.[20] As for the D_3 band, it is due to the contribution of scattering occurring in the amorphous phase,[21] which is a fully disordered structure combining carbon atoms with sp^1, sp^2, and sp^3 bonding. Finally, the D_4 band manifests itself in the spectra of carbon materials containing polyenes and ionic impurities.[22] The parameters of Raman bands and the ratios of integral intensities I_D/I_G, I_D/I_{D3}, and I_D/I_{D4} are presented in Table I. The below formula (1) permits to estimate the size L_a of sp^2 carbon clusters in the range $L_a > 2$ nm for different excitation energies E_l:[23,24]

$$L_a(\text{nm}) = \left[560/E_l^4 \times (I_D/I_G)^{-1}\right]. \quad (1)$$

Table I presents values calculated for L_a with excitation energy $E_l = 2.71$ eV. The physical meaning of the I_D/I_G ratio at the nanocluster scale can be described as follows. As the size of the carbon crystallites decreases, the role of surface defects increases as a result of the growth of the surface/volume ratio. At the same time, the number of vibrational modes caused by stretching vibrations of the internal atoms that contribute to the G-band decreases because of a smaller number of atoms inside the crystallite volumes. The sizes of carbon clusters detected in our BCMs specimens were in the range from 5.8 nm (oak-based BCM) to 10.9 nm (pear-based BCM) (Table I).

It is interesting that the averaged value of $L_a = 7.5$ nm and the averaged value of $\Gamma_G = 51$ cm^{-1} presented in Table I are in good agreement with the results,[25] where the correlation between these characteristics was investigated for a very wide range of their values. All the prepared BCMs were found to show PL with a peak at 700 nm. This indicates a possible presence of an amorphous carbon phase with C—H bonds, suggesting that all the samples had hydrogen that can passivate dangling carbon bonds (DCBs).[26] The observed PL intensity of all our samples implied that the highest content of hydrogen was in the samples obtained from pear and oak trees.

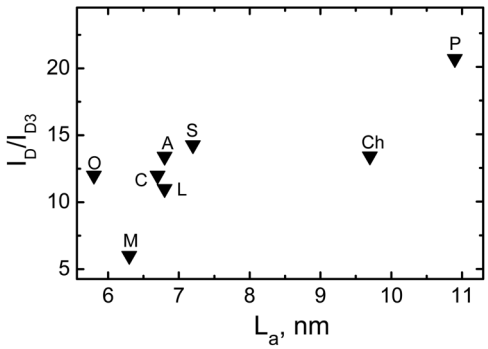

FIG. 3. Effect of cluster size L_a of graphite-like phase on the ratio I_D/I_{D3}.

Depending on precursor wood, the Raman spectra demonstrate different characteristics of their spectral components. The certain dependencies of the integral intensities ratio for Raman spectral lines I_D/I_{D3} on carbon cluster size L_a (Fig. 3) allow us to conclude which structural phase (graphite-like phase with sp^2 carbon or amorphous phase with both sp^2- and sp^3-bonds) is responsible for the structural and electronic properties of these materials.

In Fig. 3, one can see the tendency of the ratio I_D/I_{D3} to increase with the growing size of carbon nanoclusters, L_a. Although pyrolysis was carried out for all types of wood under the same conditions, analysis of the Raman spectra presented in Table I for I_D/I_{D3} shows that the percentage of the amorphous phase in them was different. In particular, the largest amorphous fraction was detected in the maple-derived BCMs (compare I_D/I_{D3} for the maple- and pear-fabricated BCMs in Fig. 3). This can be explained by the influence of different structures of the original wood, peculiarities of morphology and composition of each precursor material, whose main chemical components are cellulose, hemicelluloses, and lignin.

C. Electron spin resonance of BCMs

The same eight BCM samples described above by SEM and Raman spectroscopy (given in Table I) were studied by the ESR method. Figures 4(a)–4(c) show ESR spectra of three representative samples measured under an ambient atmosphere.

Analysis of these spectra shows that each of them is a superposition of two lines, belonging to spin systems of free and localized electron spins. They were described by the calculated functions with the Dyson-like (following the formulas[27–29]) and Lorentzian line shapes, respectively. As a result of fitting, the g-factor for both spin systems, the line width ΔB_i, and spin concentration N_s were found for each sample and are given in Table II.

It is seen from Table II that all the ESR signals (except pear-derived BCM) are very broad. The concentration of free electron spins varies considerably, $N_{ce} = (0.3–9) \times 10^{18}$ cm^{-3}. A higher N_{ce} has the BCMs from more dense and viscous wood species such as cornel, cherry-plum, and maple, but the oak-derived BCM had the lowest $N_{ce} = (2–3) \times 10^{17}$ cm^{-3} (Table II). A correlation between the concentration N_{ce} and the phase composition (which is characterized by the ratio I_D/I_{D3}) (Fig. 5) is observed.

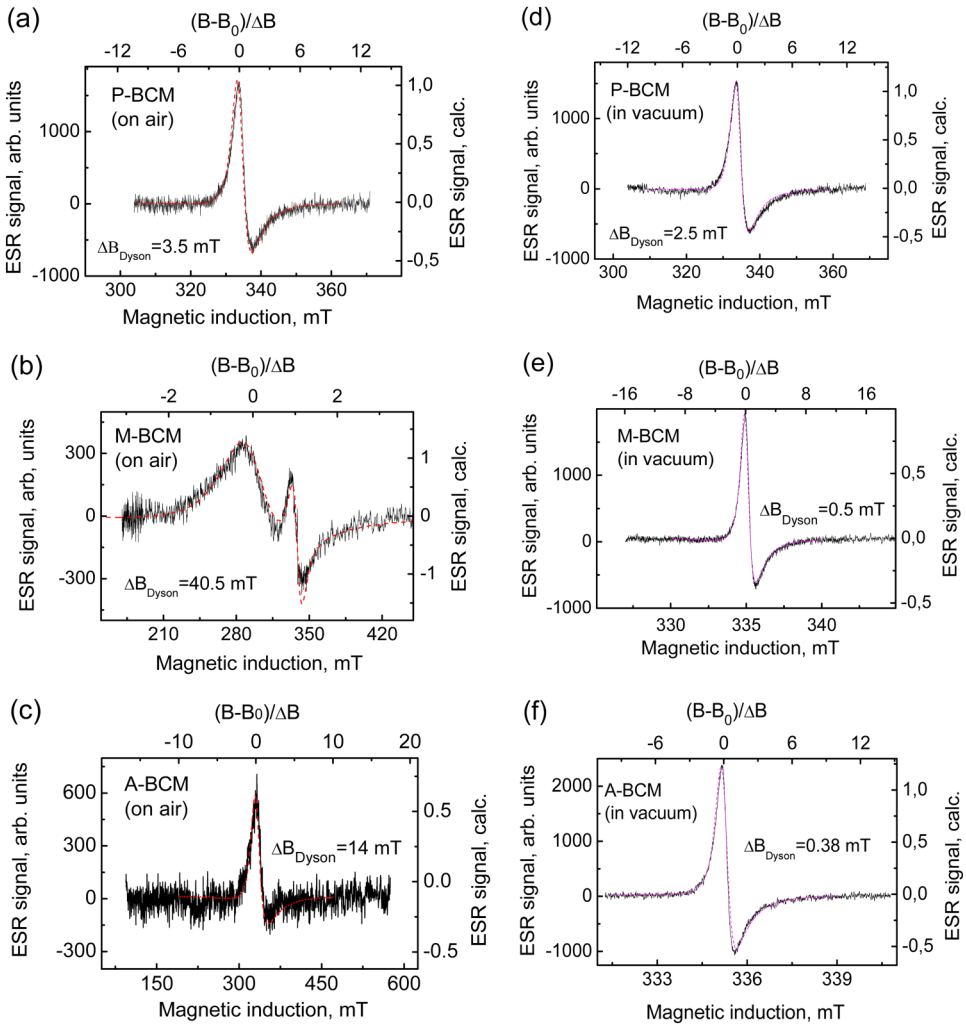

FIG. 4. [(a)–(c)] ESR spectra recorded in air for P (a), M (b), and A (c) BCM samples; [(d)–(f)] ESR spectra of the same samples under pumping out at T = 140 °C. Solid lines—experiment, dashed lines—simulated spectra in dimensionless units in accordance with the theoretical procedure for conductive samples.[27–29] In all cases, the conditions for recording the spectra were chosen to be optimal for each sample.

The free electron concentration N_e is clearly seen in Fig. 5 to decrease with the increase of the ratio I_D/I_{D3}, as a result of a decrease in the amount of amorphous phase.

1. On the origin of ESR signal in the initial BCMs and a large shift of the g-factor

Pyrolysis of biological materials leads to peculiar structural modifications of carbon. The electronic properties of the obtained BCMs have a number of features. First of all, large ESR line widths are typical for most samples stored in air [see Table II and Figs. 4(a)–4(c)]. It is due to the presence of a high amount of molecular oxygen in the pores of BCMs (for reasons, see below). Besides, a considerable negative or positive shift of g-factor from the value of 2.0023 is observed (Table II).

The signals [Figs. 4(a)–4(c)] show a high concentration of unpaired spins, including delocalized ($N_{ce} \sim 10^{18}$ cm^{-3}), therefore it is expected strongly asymmetric ESR signal with the shape of the Dyson line.[28,29] Nevertheless, the experimentally observed asymmetry of the ESR signal on air is insignificant for many samples, i.e., A/B ≤ 2, where A is a maximum and B is a minimum of ESR amplitude. At the same time, there is a noticeable negative shift in g-factor in a set of samples. The simultaneous observation of these two features implies that the asymmetry of the ESR signal has a different origin which was found for the first time in Ref. 30. When the structure of carbon frame is disordered and the crystal potential (which controls the motion of conduction electrons) fluctuates, a band of fluctuation states on which the electrons are localized appears near the bottom of the conduction band (so named "the tails of electron state density") $\rho(\varepsilon) = \rho_0 \cdot \exp(\varepsilon^2/\gamma^2)$, where γ is the distribution width of state density, ρ_0 is the pre-exponential factor, and ε is a fluctuation state energy below conduction band bottom.

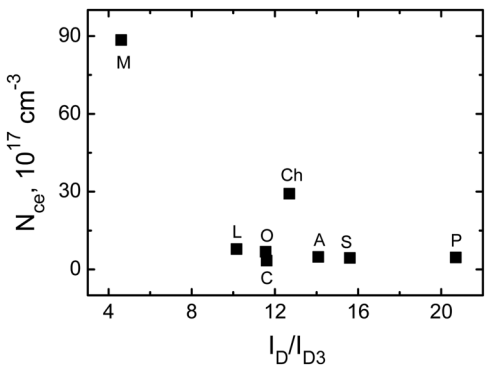

FIG. 5. Concentration of free electrons N_{ce} as a function of the ratio I_D/I_{D3}.

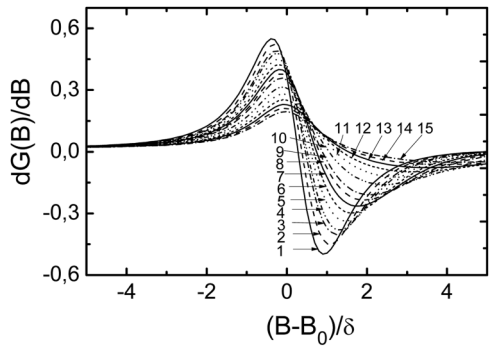

FIG. 6. Shape of the ESR line in dependence on parameter D. Curves with numbers 1–15 are calculated for the following set of D values: (1) 0.5; (2) 0.7; (3) 0.9; (4) 1.0; (5) 1.2; (6) 1.4; (7) 1.6; (8) 1.8; (9) 2.0; (10) 2.5; (11) 3.0; (12) 3.5; (13) 4.0; (14) 4.5; (15) 5.0.

Taking into account the dependence of g on ε and carrying out the above convolution, the shape of the ESR line can be expressed as the following integral:

$$G(x) = I_0 \cdot \int_{-\infty}^{D_1} d\varepsilon \exp\left(-\varepsilon^2/\gamma^2\right) \cdot \frac{1}{1 + (x + D\varepsilon/\gamma)^2}, \quad (2)$$

where $x = (B\text{-}B_0)/\delta$;

$$D = \frac{\Delta g_e \beta B_0 \cdot \gamma}{\delta \cdot E_g}, \quad (3)$$

where δ and Δg_e are the initial ESR line width and shift of g-factor in the ordered sample, respectively; $D_1 = -\varepsilon_1/\gamma$, ε_1 is the upper edge of the fluctuation level band which is equal to zero when the band begins from the conduction band bottom. The results of numerical calculations of $dG(x)/dx$ for different values D are shown in Fig. 6.

As seen in Fig. 6, the ESR signal is asymmetric, i.e., the derivative of absorption has the maximum amplitude value A bigger than the minimum value B. The ratio A/B depends on the value of the parameter D (Fig. 7). As far as in our experimental ratio $A/B \leq 2$, from Fig. 7 follows the D value to be limited by $D \leq 2.5$. The estimation of D in Eq. (2) with $g = 1.94$ for the L type BCM (see Table II) gives $D = 2$ when the width of the fluctuation state band $\gamma \approx 0.05 \cdot E_g$, which is reasonable for graphite-like carbon systems. So the simultaneous observation of an asymmetric ESR signal with a large

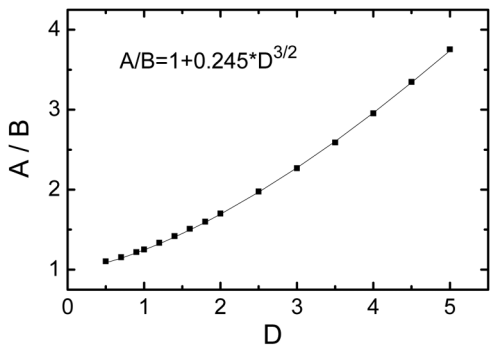

FIG. 7. Dependence of the asymmetry factor (A/B) on parameter D. A is the maximum; B is the minimum of the ESR signal derivative.

width and a large negative shift of g-factor ($g < 2.0023$) points at the presence of a graphite-like structure with a sufficiently wide band of fluctuation states and the narrow gap.

In evacuated BCM samples, the value of N_e can change by several times (Table II). All samples are still characterized by spectra [Figs. 4(d)–4(f)], which is a sum of two overlapping signals, i.e., conduction electron spin resonance (CESR) and a Lorentz shape signal of localized spins belonging to the DCBs. The ESR line width in all evacuated BCMs, except the pear- and oak-derived BCMs, drastically reduced by a factor of 2.5–100 (Table II).

Among all the evacuated BCMs, one group of them (A, O, L, and M BCM) is characterized by $g = 2.0006$–2.0034 (typical for DCBs) and relatively small ESR line width $\Delta B = 0.1$–1 mT. Another group (Ch, S, P, and O sapwood BCMs) is characterized by a significant g-shift and more broad ESR line width under pumping out (Table II). The reasons for this behavior will be discussed below.

2. Effect of adsorbed oxygen

A large ESR line width is typical for BCM samples stored in the ambient atmosphere. The reason for this is the dipole-dipole interaction between electron spins and spins of oxygen molecules, which is known to cause a remarkable increase of the ESR line width proportional to the concentration of the adsorbed oxygen.[31]

After pumping out the oxygen, ESR signals were found to be abruptly narrowed for most of the samples (see Table II). The preservation of a wide ESR line after pumping out in some samples (BCMs from sea-buckthorn, pear, and oak sapwood) can be explained by the existence of closed pores where oxygen molecules are preserved. One can suppose, the BCM sample fabricated from oak sapwood, which has the widest ESR line under pumping out ($\Delta B_{pp} \sim 48$ mT), has numerous closed pores in its structure. Another remarkable sample is the pear-derived BCMs having a minimum fraction of amorphous structure (maximum I_D/I_{D3}). The smallest among all samples of ESR line width in air and the invariance of it on pumping out indicate a small total pore surface in pear BCM and approximately an equal number of oxygen molecules in open and closed pores.

Since molecular oxygen affects the line width and integral intensity of the ESR spectrum there is a possibility to control the surface behavior of oxygen during adsorption or reaction. A similar behavior was observed for certain types of carbon nanostructures.[32,33]

IV. SIC CERAMICS: RESULTS AND DISCUSSION

A. SEM images

Of all the BCM samples prepared in this study, two of the most typical ones were chosen for the preparation of SiC ceramics. The first is the alder-derived BCMs. It has a good open porosity (roughly tested by the difference in the ESR line widths in air and in the evacuated state) and a significant concentration of free electrons independent of treatments (see Table II). All the alder-derived BCM samples are good candidates for converting them to SiC ceramic material.

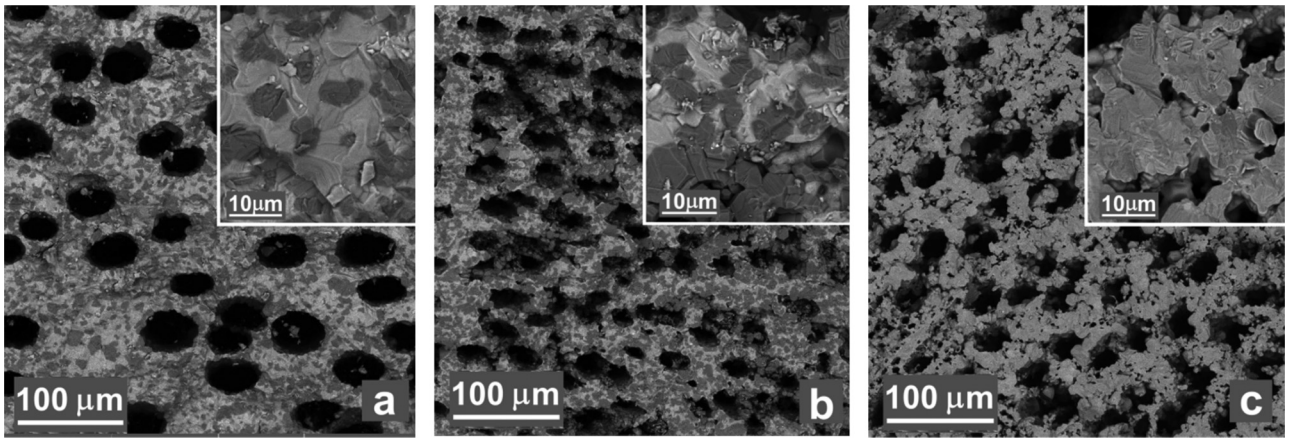

FIG. 8. SEM images of SiC ceramic samples Ac, Pc1, and Pc2 formed from alder- (a) and pear- [(b) and (c)] derived BCMs, accordingly. The insets show enlarged images of sections of the same structures on which the composition of the elements was determined by energy dispersive X-ray elemental analysis (EDX) (furthermore, they are given in at. %). (a) C = 75, Si = 25 (dark spots), C = 35, Si = 65 (light spots); (b) C = 60, Si = 40 (dark spots), C = 18, Si = 82 (light spots); (c) C = 58, Si = 42.

Furthermore, oak refers to hard and viscous tree species, but BCMs from it appeared to have very low values of open porosity. In this regard, pear-based BCMs (also hard and viscous trees, but with a significantly higher open porosity BSM) were chosen for silicon impregnation. Figure 8 shows the SEM images and displays the EDX data of SiC ceramic samples Ac, Pc1, and Pc2a.

It is well seen in Fig. 8 that after reaction with liquid Si small pores with sizes of 1–10 μm mainly disappeared in the produced SiC ceramics, while larger pores ($\sim$ 20 μm in size) are well observed. It is seen also that samples Ac and Pc1 prepared at temperatures $T_{impr.} = 1700$ and $T_{impr.} = 1900$ °C, respectively, have a stronger heterogeneity of the elemental composition compared to sample Pc2, which was synthesized at T = 1950 °C and it is practically homogeneous. In addition, it can be seen that only pores of large sizes ($\sim$20 μm) remain open in all samples.

B. Raman scattering

Raman spectra of both Ac and Pc type SiC ceramic samples, prepared at different impregnation temperatures (T_{impr}), are presented in Fig. 9. All spectra are seen to have a band of residual silicon in the frequency range from 522 to 539 cm^{-1}, a TO-band of SiC ceramics at $\sim$800 cm^{-1}, and wide bands at 950 and 1520 cm^{-1} which are the second-order bands of optical phonons of silicon and SiC, respectively. The intensities of the latter bands were found to depend on the kind of BCM, the amount of residual silicon, and on the T_{impr}.

In the Raman spectrum of the sample Ac, Fig. 9(a), the shape and position of the TO band with a maximum at 801 cm^{-1} proves that under the selected conditions ($T_{impr.}$ = 1700 °C, C/Si $\leq$ 2.33) a cubic (3C) SiC polytype was formed. It is also seen in Fig. 9(a) that in addition to the SiC band, a band of silicon with a frequency of 525 cm^{-1} is also present. A slight shift of the band to higher frequencies compared with the well-known values (521–522 cm^{-1}) indicates that silicon has compressive stress.

Figure 9(b) shows the Raman spectra of SiC ceramic samples obtained from the pear derived BCMs at $T_{impr.}$ = 1900 (Pc1) and 1950 °C (Pc2a, Pc2b). The samples Pc2a and Pc2b were cut out from the surface and inner parts of one large piece of SiC ceramics, respectively. The sample Pc1 synthesized at 1900 °C exhibits a silicon band and the band at 523 cm^{-1}, the latter band is an order of magnitude greater than the intensity of the TO band of SiC at 797 cm^{-1}. This indicates that the sample Pc1 formed at 1900 °C had a relatively high amount of residual Si, similar to the Ac sample in Fig. 9(a). An increase in temperature to 1950 °C is seen to result in a significant decrease in the amount of silicon and an increase of the SiC phase in the product [spectra of samples Pc2a and Pc2b in Fig. 9(b)]. In addition, in spectra Pc2a and Pc2b, the LO bands of SiC and a series of second-order SiC bands become visible and several bands appear in

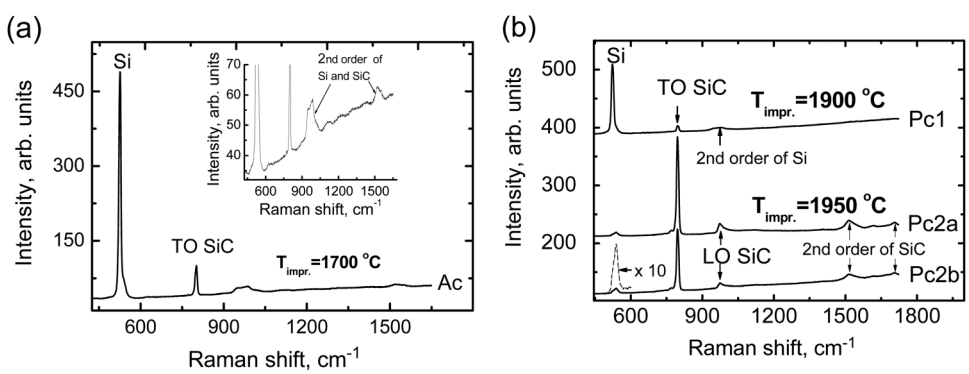

FIG. 9. Raman spectra of SiC ceramic samples Ac, Pc1, Pc2a, and Pc2b, synthesized on base of alder- (a) and pear- (b) derived BCMs. The inset in Fig. 9(a) shows enlarged second-order bands of Si and SiC. Samples Pc2a and Pc2b in Fig. 9(b) were cut out from the surface and inner parts of one large piece of SiC ceramics, respectively.

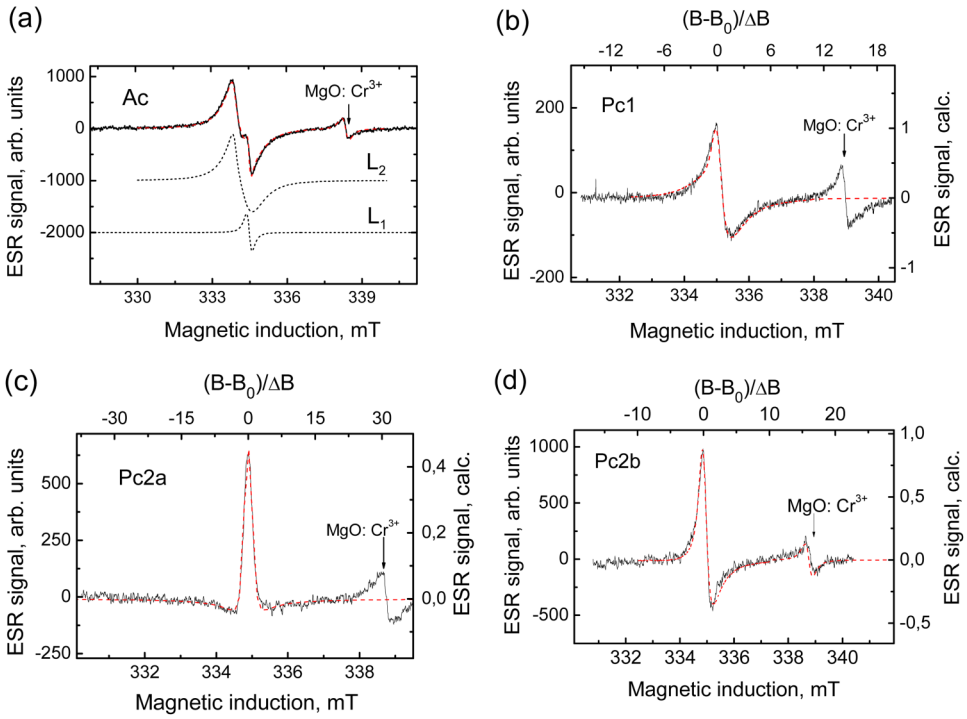

FIG. 10. ESR spectra of SiC ceramic samples Ac (a), Pc1 (b), Pc2a (c), and Pc2b (d). Solid lines present experimental data, while dashed lines stand for simulated spectra (for samples Pc1, Pc2a, Pc2b, they are calculated in accordance with the theoretical procedure for conductive materials).[27–29]

the region of Si-Si oscillations (the most high-frequency of them is about 539 cm^{-1}), in contrast to bulk and no stressed Si (~520 cm^{-1}). These features can be prescribed to a big biaxial compression of residual silicon caused by the SiC matrix. This leads to the splitting of the F_{2g} mode into a singlet and doublet and their shift in the high-frequency side. Another possible reason for the appearance of these bands is due to the formation of a solid solution of $C_xSi_{1-x}O_2$, which was discussed in Ref. 34. The intensity ratio I_{SiC}/I_{Si} for the sample Pc2a in Fig. 9(b) is greater than the corresponding ratio for the sample Pc2b. This can be explained by the variation of the porous structure that varied somewhat in different parts of the same BCM sample, which in turn affected the impregnation of the carbon matrix with liquid silicon.

C. Electron spin resonance

The ESR spectra of the same SiC ceramics samples were measured, with the results being presented in Fig. 10.

The spectrum of the Ac sample [Fig. 10(a)] can be described as a sum of two lines, L_1 and L_2. The line L_1 is characterized by g = 2.0028 and ΔB = 0.13 mT, while the line L_2 is the result of computer simulation of ESR signal with a Lorentz line shape and anisotropic g-factor and line width. The simulation includes the averaging of the Lorentzian function on angles θ, φ between the magnetic field and the main axes of the g-tensor. The parameters of both lines L_1 and L_2 are given in Table III.

The ESR spectra in Figs. 10(b)–10(d) (samples Pc1, Pc2a, Pc2b) refer to the SiC samples prepared from pear-derived BCMs. The parameters of these samples theoretically calculated following procedures previously developed in Refs. 27–29 for conductive materials are given in Table IV.

Comparison of the data presented in Tables III and IV with those for BCMs (Table II) shows that in SiC ceramics values of N_s decrease 3–80 times, which is not surprising since the sample structure changed completely. Furthermore, after treatment of BCMs with liquid Si, not only the structure but also the open porosity of the prepared SiC samples changed drastically. As SEM images in Fig. 8 show, mainly macro pores remained in the final product, while the majority of small closed pores disappeared. As a result, as seen in Fig. 10, oxygen from the air had almost no effect on the observed ESR line width of ceramic SiC samples.

Let us now discuss the nature of the paramagnetic centers. In the Ac sample ESR line L_1 ($N_{L1} = 3 \cdot 10^{15}$ cm^{-3}) has isotropic g-factor g = 2.0028, the narrow line width ΔB = 0.13 mT, and can be reliably attributed to DCBs at the interface C/SiC.[35] Components of the g-tensor for signal L_2 points onto the absence of Si dangling bonds (DB), because

TABLE III. Characteristics of the ESR lines of alder-derived SiC ceramics sample Ac.

Line	$g_{\parallel}$	$g_{\perp}$	$\Delta B_{\parallel}$ mT	$\Delta B_{\perp}$ mT	N_s (10^{16} cm^{-3})
L_1	2.0028	2.0028	0.13	0.13	0.3
L_2	2.0064	2.0037	0.14	0.8	13

TABLE IV. Characteristics of the ESR signals of pear-derived SiC ceramics samples.

Sample	ESR signal	g-value	ΔB (mT)	N_s (10^{16} cm^{-3})
Pc1	Free carriers	2.0032	0.27	0.3
	Localized PC	2.0032	0.82	0.6
Pc2a	Free carriers	2.0027	0.13	0.4
Pc2b	Free carriers	2.0036	0.24	5.4
	Localized PC	2.0036	0.48	2.2

the g-tensor of all kinds of Si DBs shows $g_{\parallel} < g_{\perp}$[36,37]. The inverse relationship $g_{\parallel} > g_{\perp}$ is observed for carbon vacancies.[38,39] Thus, the negatively charged vacancy V_C^- has $g_{\parallel} = 2.0040$, $g_{\perp} = 2.0038$ in 4H SiC in the hexagonal position,[40] and the positive one V_C^+ has $g_{\parallel} = 2.0060$, $g_{\perp} = 2.0026$ in 6H SiC for the quasi-cubic position; and the same is expected in 3C SiC.[37] Therefore, it is most probable that signal L_2 ($N_{L2} = 1.3 \cdot 10^{17}\ cm^{-3}$) belongs to the positively charged carbon vacancies. The fact that the values of $g_{\parallel}$ and $g_{\perp}$ were found to be somewhat larger than those predicted earlier in Ref. 36 can be explained by the presence of compressive stress that resulted from the quenching of excessive silicon, which also agrees with the Raman data discussed above.

ESR signals in the Pc samples differ in the set of samples Pc1, Pc2a, and Pc2b. Signals in the samples Pc1 and Pc2b [Figs. 10(b) and 10(d)] show the typical combination of the Dysonian line shape for free electron and Lorentzian line shape for the DCBs with parameters given in Table IV and typical for signals in BCMs, but much lower intensity. Although the amount of the residual carbon is not enough for the observation in Raman spectra, it is enough to be revealed in ESR spectra. As for the sample Pc2a [Fig. 10(c)], which was cut off the surface part of a larger SiC piece, its ESR spectrum demonstrates only free electrons signal with a special line shape like the second derivative of the absorption. Such a shape of the ESR signal can be observed only under certain conditions: the material has a noticeable concentration of free electrons, high conductivity, and high rate of electron diffusion. From the theory in Refs. 27–29, it follows that under such conditions, the signal is described by the following equation:

$$f(B) = I_0 \cdot \frac{d}{dB}\left[\frac{B - B_{res}}{|B - B_{res}|} \cdot \frac{\{[1 + (B - B_{res})^2 T_2^2]^{1/2} - 1\}^{1/2}}{[1 + (B - B_{res})^2 T_2^2]^{1/2}}\right]. \quad (4)$$

The ESR spectrum of the sample Pc2a in Fig. 10(c) is described by Eq. (4) with parameters $B_{res} = 334.88$ mT (which corresponds to $g = 2.0028$) and $T_2 = 1.48 \cdot 10^{-7}$ s. The above value can be realized for the well conductive material. Two fractions of sample Pc2a, namely, Si and SiC, being undoped by donors, have not high conductivity. Only a thin layer of graphite-like carbon can be responsible for this ESR signal. The ESR spectrum of the sample Pc2a shows also the absence of any defects in addition to free electrons. Specializing experiments using four additional samples (Pc2c-Pc2f) cut from the same large piece of pear-derived SiC ceramic as samples Pc2a and Pc2b showed a high structure uniformity of the big SiC ceramic piece (the ratio I_{SiC}/I_{Si} does not change more than by a factor of 2 for samples Pc2a-Pc2f). Moreover, within the Pc2a-Pc2f sample set, the increase in the I_{SiC}/I_{Si} ratio correlates with a decrease in the concentration of defects and free electrons in the sample, thus establishing a connection between structural excellence and electronic characteristics of the ceramic.

V. CONCLUSIONS

So far, detailed studies on the electron paramagnetic resonance were not performed for the biomorphic carbon matrices as was for bio-SiC ceramics. At the same time, as our research shows, the electronic structure of BCMs predetermines in many respects the physical properties of the final product. A large number of dangling carbon bonds support the successful interaction of liquid silicon and the carbon system, and ESR is a perfect indicator of the electronic properties of the material.

BCMs were produced by pyrolysis from wood species of different forest and garden trees, after which the prepared BCMs were converted into SiC ceramics by impregnating with liquid silicon at $T_{impr.} = 1700$–1950 °C. Morphologically, all the BCMs contain large (10–50 μm) and small (1–5 μm) pores with surface density $\sim 10^9\ m^{-2}$ and $10^{11}\ m^{-2}$, respectively. They contain nanocrystalline carbon with sizes of clusters ~5–10 nm, which manifested in the characteristics of the G- and D-bands of the Raman spectra. The electronic properties of BCMs, established by the electron spin resonance method, are due to the contributions of three spin systems: free electron spins, "pseudo-free" spins from the tails of density states below the conduction band, and localized spins at the dangling carbon bonds. We have established that a set of features of the observed ESR signals in the initial BMC, namely, a weak asymmetry and a significant negative shift of the g-factor, make it possible to state that the electrons are not completely free, but localized on potential fluctuations. The width of the ESR lines, which is very large in the ambient air, drastically narrows when the samples are pumped out, due to the exclusion of the interaction with molecular oxygen.

Impregnation of BCMs with silicon leads to the formation of a SiC ceramics (3C polytype), the structural and electronic properties of which depend on the type of the original matrix and T_{impr}. SEM, Raman, and ESR studies of the obtained SiC ceramics showed that the most high-quality samples with the maximum contribution of the SiC phase and the maximum homogeneity of its distribution over the big workpiece (~10 cm^3) were achieved using a pear-based BCM and $T_{impr} = 1950$ °C. Samples of this ceramics are also characterized by a negligible excess of silicon and a low concentration of paramagnetic defects. Free electrons demonstrate the specific shape of the ESR line in such ceramics, which is due to the high conductivity of the remaining graphite-like nanoclusters. One can assume that it is possible to control the electronic properties of bioceramics by controlling the content of graphite-like nanoclusters in it. After the impregnation with silicon, the potential fluctuations are eliminated, and the silicon carbide ceramics turns out to be almost defect-free.

Finally, it should be noted that controlling the synthesis of a biomorphic SiC with a definite polytype (cubic or hexagonal) is relatively easier than in other methods. Only two factors—the ratio of silicon and carbon content and the temperature—determine the crystal structure, and random factors are absent.

ACKNOWLEDGMENTS

The authors of the paper are grateful for support by National Academy of Science of the Ukraine (Project No. 26/18-H).

[1]M. I. Kairi, M. Khavarian, S. A. Bakar, B. Vigolo, and A. R. Mohamed, J. Mater Sci. **53**, 851 (2018).
[2]C. Sanchez, H. Arrbart, and M. M. G. Giraud, Nat. Mater. **4**, 277 (2005).
[3]V. S. Kiselov, P. M. Lytvyn, V. O. Yukhymchuk, A. E. Belyaev, and S. A. Vitusevich, J. Appl. Phys. **107**, 093510 (2010).
[4]V. O. Yukhymchuk, V. S. Kiselov, M. Y. Valakh, M. P. Tryus, M. A. Skoryk, A. G. Rozhin, S. A. Kulinich, and A. E. Belyaev, J. Phys. Chem. Solids. **91**, 145 (2016).
[5]F. Eichhorn, A. Stenzel, B. Weisenseel, N. Travitzky, K. Kakimoto, P. Greil, and T. Fey, Mater Lett. **206**, 158 (2017).
[6]Q. Liu, J. Gu, W. Zhang, Y. Miyamoto, Z. Chen, and D. Zhang, J. Mater Chem. **22**(39), 21183 (2012).
[7]F. Cazana, A. Galetti, C. Meyera, V. Sebastián, M. A. Centeno, E. Romeo, and A. Monzon, Catal. Today **301**, 226 (2018).
[8]P. W. Xiao, Q. Meng, L. Zhao, J. J. Li, Z. Wei, and B. H. Han, Mater Design. **129**, 164 (2018).
[9]F. Chen, A. S. Gong, M. Zhu, G. Chen, S. D. Lacey, F. Jiang, Y. Li, Y. Wang, J. Dai, Y. Yao, J. Song, B. Liu, K. Fu, S. Das, and L. Hu, ACS Nano. **11**, 4275 (2017).
[10]J. S. Lee, H. J. Lee, J. M. Yoo, T. Kim, and Y. H. Kim, ACS Appl. Mater Interfaces. **9**, 43959 (2017).
[11]M. Broda and M. Frankowski, Environ Sci. Pollut. Res. **24**, 23401 (2017).
[12]Y. Cheng, K. Feng, H. Q. Wang, H. Z. Zhang, X. F. Li, and H. M. Zhang, Adv. Mater Interfaces. **4**, 1700686 (2017).
[13]M. Inagaki, H. Konno, and O. Tanaike, J. Power Sources. **195**(24), 7880 (2010).
[14]G. Lalwani, S. C. Patel, and B. Sitharaman, Ann. Biomed. Eng. **44**(6), 2020–35 (2016).
[15]T. C. Wang, L. J. Chang, S. Yang, Y. Jia, and C. P. Wong, Ceram. Int. **39**, 8165 (2013).
[16]J. Will, A. Hoppe, F. A. Müller, C. T. Raya, J. M. Fernandez, and P. Greil, Acta Biomater. **6**, 4488 (2010).
[17]M. Es-Souni, D. Schopf, C. H. Solterbeck, and M. Dietze, RSC Adv. **4**, 17748 (2014).
[18]S. Reich and C. Thomsen, Phil. Trans. R. Soc. Lond. A **362**, 2271 (2014).
[19]A. C. Ferrari and J. Robertson, Phys. Rev. B **61**, 14095 (2000).
[20]V. O. Yukhymchuk, M. Y. Valakh, O. M. Hreshchuk, Y. O. Havrylyuk, I. B. Yanchuk, A. V. Yefanov, R. N. Arif, A. G. Rozhin, and M. A. Skoryk, Ukr. J. Phys. **62**(5), 432 (2017).
[21]S. Ravi and P. Silva, *Properties of Amorphous Carbon* (INSPEC IEE, London, UK, 2003).
[22]A. Sadezky, H. Muckenhuber, H. Grothe, R. Niessner, and U. Poschl, Carbon. **43**, 1731 (2005).
[23]L. G. Cancado, K. Takai, T. Enoki, M. Endo, Y. A. Kim, H. Mizusaki, A. Jorio, L. N. Coelho, R. Magalhaes-Paniago, and M. A. Pimenta, Appl. Phys. Lett. **88**, 163106 (2006).
[24]F. Tuinstra and J. L. Koening, J. Chem. Phys. **53**, 1126 (1970).
[25]J. Ribeiro-Soares, M. E. Oliveros, C. Garin, M. V. David, L. G. P. Martins, C. A. Almeida, E. H. Martins-Ferreira, K. Takai, T. Enoki, R. Magalhaes-Paniago, A. Malachias, A. Jorio, B. S. Archanjo, C. A. Achete, and L. G. Cancado, Carbon. **95**, 646 (2010).
[26]C. Casiraghi, A. C. Ferrari, and J. Robertson, Phys. Rev. B. **72**, 085401 (2005).
[27]G. Feher and A. F. Kip, Phys. Rev. **98**, 337 (1955).
[28]J. H. Pifer and R. Magno, Phys. Rev. B. **3**, 663 (1971).
[29]V. G. Gavriljuk, S. P. Efimenko, Y. E. Smuk, S. U. Smuk, B. D. Shanina, N. P. Baran, and V. M. Maksimenko, Phys. Rev. B. **48**, 3224 (1993).
[30]V. M. Babich, N. P. Baran, A. A. Bugai, A. A. Konchits, V. B. Kovalchuk, V. M. Maksimenko, and B. D. Shanina, Phys. Stat. Sol. A. **109**, 537 (1988).
[31]O. Y. Grinberg, B. B. Williams, A. E. Runge, S. E. Grinberg, D. F. Wilcox, H. M. Swarts, and J. H. Freed, J. Phys. Chem. B. **111**, 13316 (2007).
[32]A. R. Chughtai, M. M. O. Atteya, J. Kim, B. K. Konowalchuk, and D. M. Smith, Carbon **36**(11), 1573 (1998).
[33]A. A. Konchits, B. D. Shanina, M. Y. Valakh, I. B. Yanchuk, V. O. Yukhymchuk, A. D. Alexeev, T. A. Vasilenko, A. N. Molchanov, and A. K. Kirillov, J. Appl. Phys. **112**, 043504 (2012).
[34]M. Santoro, F. A. Gorelli, R. Bini, A. Salamat, G. Garbarino, C. Levelut, O. Cambon, and J. Haines, Nat. Commun. **7**, 13538 (2016).
[35]H. J. Von Bardeleben, J. L. Cantin, M. Mynbaeva, S. E. Saddow, Y. Shishkin, R. P. Devaty, and W. J. Choyke, *Silicon Nitride Silicon Dioxide Thin Insulating Films VII: Proceedings Series* (2003), Vol. 2, p. 39.
[36]K. Morigaki, C. Niikura, H. Hikita, and M. Yamaguchi, J. App. Phys. **105**, 083703 (2009).
[37]K. Morigaki and C. Niikura, Solid State Commun. **136**, 308 (2005).
[38]G. Gruber, P. Hadley, M. Koch, D. Peters, and T. Aichinger, AIP Conf. Proc. **1583**, 165 (2014).
[39]T. Umeda, Y. Ishitsuka, J. Isoya, N. T. Sonand, E. Janzen, N. Morishita, T. Ohshima, H. Itoh, and A. Gali, Phys. Rev. B. **71**, 193202 (2005).
[40]V. Y. Bratus, T. T. Petrenko, S. M. Okulov, and T. L. Petrenko, Phys. Rev. B. **71**, 125202 (2005).